Effect of the size and shape of a red blood cell on elastic light scattering properties at the single-cell level

Matti Kinnunen,[1,*] Antti Kauppila,[1] Artashes Karmenyan,[2] and Risto Myllylä[1]

[1]*Optoelectronics and Measurement Techniques Laboratory, University of Oulu, Finland*
[2]*Institute of Biophotonics, National Yang-Ming University, Taipei, Taiwan*
*matti.kinnunen@ee.oulu.fi

Abstract: We demonstrate the use of a double-beam optical tweezers system to stabilize red blood cell (RBC) orientation in the optical tweezers during measurements of elastic light scattering from the trapped cells in an angle range of 5-30 degrees. Another laser (He-Ne) was used to illuminate the cell and elastic light scattering distribution from the single cell was measured with a goniometer and a photomultiplier tube. Moreover, CCD camera images of RBCs with and without laser illumination are presented as complementary information. Light scattering from a RBC was measured in different fixed orientations. Light scattering from cells was also measured when the length of the cell was changed in two different orientations. Light scattering measurements from spherical and crenate RBCs are described and the results are compared with other cell orientations. Analysis shows that the measured elastic light scattering distributions reveal changes in the RBC's orientation and shape. The effect of stretching on the changes in scattering is larger in the case of face-on incidence of He-Ne laser light than in rim-on incidence. The scattering patterns from RBCs in different orientations as well as from a spherical RBC were compared with numerical results found in literature. Good correlation was found.

OCIS codes: (350.4855) Optical tweezers or optical manipulation; (290.5850) Scattering, particles; (170.1530) Cell analysis.

References and links:

1. Y. Park, M. Diez-Silva, D. Fu, G. Popescu, W. Choi, I. Barman, S. Suresh, and M. S. Feld, "Static and dynamic light scattering of healthy and malaria-parasite invaded red blood cells," J. Biomed. Opt. **15**(2), 020506 (2010).
2. K. Bambardekar, J. A. Dharmadhikari, A. K. Dharmadhikari, T. Yamada, T. Kato, H. Kono, Y. Fujimura, S. Sharma, and D. Mathur, "Shape anisotropy induces rotations in optically trapped red blood cells," J. Biomed. Opt. **15**(4), 041504 (2010).
3. M. Friebel, J. Helfmann, and M. C. Meinke, "Influence of osmolarity on the optical properties of human erythrocytes," J. Biomed. Opt. **15**(5), 055005 (2010).
4. Ö. Ergül, A. Arslan-Ergül, and L. Gürel, "Computational study of scattering from healthy and diseased red blood cells," J. Biomed. Opt. **15**(4), 045004 (2010).
5. S. V. Tsinopoulos and D. Polyzos, "Scattering of he-ne laser light by an average-sized red blood cell," Appl. Opt. **38**(25), 5499–5510 (1999).
6. D. H. Tycko, M. H. Metz, E. A. Epstein, and A. Grinbaum, "Flow-cytometric light scattering measurement of red blood cell volume and hemoglobin concentration," Appl. Opt. **24**(9), 1355–1365 (1985).
7. A. M. K. Nilsson, P. Alsholm, A. Karlsson, and S. Andersson-Engels, "T-matrix computations of light scattering by red blood cells," Appl. Opt. **37**(13), 2735–2748 (1998).
8. J. He, A. Karlsson, J. Swartling, and S. Andersson-Engels, "Light scattering by multiple red blood cells," J. Opt. Soc. Am. A **21**(10), 1953–1961 (2004).
9. A. Karlsson, J. He, J. Swartling, and S. Andersson-Engels, "Numerical simulations of light scattering by red blood cells," IEEE Trans. Biomed. Eng. **52**(1), 13–18 (2005).
10. Y. R. Kim and L. Ornstein, "Isovolumetric sphering of erythrocytes for more accurate and precise cell volume measurement by flow cytometry," Cytometry **3**(6), 419–427 (1983).

11. A. N. Shvalov, J. T. Soini, A. V. Chernyshev, P. A. Tarasov, E. Soini, and V. P. Maltsev, "Light-scattering properties of individual erythrocytes," Appl. Opt. **38**(1), 230–235 (1999).
12. A. G. Borovoi, E. I. Naats, and U. G. Oppel, "Scattering of light by a red blood cell," J. Biomed. Opt. **3**(3), 364–372 (1998).
13. K. A. Sem'yanov, P. A. Tarasov, J. T. Soini, A. K. Petrov, and V. P. Maltsev, "Calibration-free method to determine the size and hemoglobin concentration of individual red blood cells from light scattering," Appl. Opt. **39**(31), 5884–5889 (2000).
14. M. A. Yurkin, K. A. Semyanov, P. A. Tarasov, A. V. Chernyshev, A. G. Hoekstra, and V. P. Maltsev, "Experimental and theoretical study of light scattering by individual mature red blood cells by use of scanning flow cytometry and a discrete dipole approximation," Appl. Opt. **44**(25), 5249–5256 (2005).
15. H. Ding, Z. Wang, F. Nguyen, S. A. Boppart, and G. Popescu, "Fourier transform light scattering of inhomogeneous and dynamic structures," Phys. Rev. Lett. **101**(23), 238102 (2008).
16. M. Bartholdi, G. C. Salzman, R. D. Hiebert, and M. Kerker, "Differential light scattering photometer for rapid analysis of single particles in flow," Appl. Opt. **19**(10), 1573–1581 (1980).
17. A. Brunsting and P. F. Mullaney, "Differential light scattering from spherical mammalian cells," Biophys. J. **14**(6), 439–453 (1974).
18. K. Ramser and D. Hanstorp, "Optical manipulation for single-cell studies," J Biophotonics **3**(4), 187–206 (2010).
19. K. König, H. Liang, M. W. Berns, and B. J. Tromberg, "Cell damage by near-IR microbeams," Nature **377**(6544), 20–21 (1995).
20. K. König, H. Liang, M. W. Berns, and B. J. Tromberg, "Cell damage in near-infrared multimode optical traps as a result of multiphoton absorption," Opt. Lett. **21**(14), 1090–1092 (1996).
21. J. P. Mills, L. Qie, M. Dao, C. T. Lim, and S. Suresh, "Nonlinear elastic and viscoelastic deformation of the human red blood cell with optical tweezers," Mech. Chem. Biosyst. **1**(3), 169–180 (2004).
22. R. C. Gauthier, M. Ashman, and C. P. Grover, "Experimental confirmation of the optical-trapping properties of cylindrical objects," Appl. Opt. **38**(22), 4861–4869 (1999).
23. S. C. Grover, R. C. Gauthier, and A. G. Skirtach, "Analysis of the behaviour of erythrocytes in an optical trapping system," Opt. Express **7**(13), 533–539 (2000).
24. S. Sato, M. Ishigure, and H. Inaba, "Optical trapping and rotational manipulation of microscopic particles and biological cells using higher order mode Nd: YAG laser beams," Electron. Lett. **27**(20), 1831–1832 (1991).
25. G. B. Liao, P. B. Bareil, Y. Sheng, and A. Chiou, "One-dimensional jumping optical tweezers for optical stretching of bi-concave human red blood cells," Opt. Express **16**(3), 1996–2004 (2008).
26. A. Kauppila, M. Kinnunen, A. Karmenyan and R. Myllylä are preparing a manuscript to be called "Design and implementation of a system for cell manipulation using various methods in free suspension."
27. W. H. Wright, G. J. Sonek, Y. Numajiri, and M. W. Berns, "Measurement of light scattering from cells using an inverted infrared optical trap," Proc. SPIE **1427**, 279–287 (1991).
28. D. Watson, N. Hagen, J. Diver, P. Marchand, and M. Chachisvilis, "Elastic light scattering from single cells: orientational dynamics in optical trap," Biophys. J. **87**(2), 1298–1306 (2004).
29. R. M. P. Doornbos, M. Schaeffer, A. G. Hoekstra, P. M. A. Sloot, B. G. Grooth, and J. Greve, "Elastic light-scattering measurements of single biological cells in an optical trap," Appl. Opt. **35**(4), 729–734 (1996).
30. M. Collins, A. Kauppila, A. Karmenyan, L. Gajewski, K. Szewczyk, M. Kinnunen, and R. Myllylä, "Measurement of light scattering from trapped particles," Proc. SPIE **7376**, 737619, 737619-8 (2010).
31. K. Ramser, K. Logg, M. Goksör, J. Enger, M. Käll, and D. Hanstorp, "Resonance Raman spectroscopy of optically trapped functional erythrocytes," J. Biomed. Opt. **9**(3), 593–600 (2004).
32. L. Peng, D. Chen, P. Setlow, and Y. Q. Li, "Elastic and inelastic light scattering from single bacterial spores in an optical trap allows the monitoring of spore germination dynamics," Anal. Chem. **81**(10), 4035–4042 (2009).
33. Z. J. Smith and A. J. Berger, "Validation of an integrated Raman- and angular-scattering microscopy system on heterogeneous bead mixtures and single human immune cells," Appl. Opt. **48**(10), D109–D120 (2009).
34. A. Roggan, M. Friebel, K. Dörschel, A. Hahn, and G. Müller, "Optical properties of circulating human blood in the wavelength range 400-2500 nm," J. Biomed. Opt. **4**(1), 36–46 (1999).
35. P. Mazeron, S. Muller, and H. el Azouzi, "Deformation of erythrocytes under shear: a small-angle light scattering study," Biorheology **34**(2), 99–110 (1997).
36. P. Galajda and P. Ormos, "Orientation of flat particles in optical tweezers by linearly polarized light," Opt. Express **11**(5), 446–451 (2003).
37. S. K. Mohanty, K. S. Mohanty, and P. K. Gupta, "Dynamics of Interaction of RBC with optical tweezers," Opt. Express **13**(12), 4745–4751 (2005).
38. P. Laven, "MiePlot: a computer program for scattering of light from a sphere using Mie theory & the Debye series," http://www.philiplaven.com/mieplot.htm
39. G. J. Streekstra, A. G. Hoekstra, E.-J. Nijhof, and R. M. Heethaar, "Light scattering by red blood cells in ektacytometry: Fraunhofer versus anomalous diffraction," Appl. Opt. **32**(13), 2266–2272 (1993).
40. E. Fällman and O. Axner, "Design for fully steerable dual-trap optical tweezers," Appl. Opt. **36**(10), 2107–2113 (1997).
41. V. V. Tuchin, "Optical immersion as a new tool for controlling the optical properties of tissues and blood," Laser Phys. **15**, 1109–1136 (2005).
42. A. A. Bednov, E. V. Savateeva, and A. A. Oraevsky, "Glucose monitoring in whole blood by measuring laser-induced acoustic profiles," Proc. SPIE **4960**, 21–29 (2003).

43. S. Rao, S. Bálint, B. Cossins, V. Guallar, and D. Petrov, "Raman study of mechanically induced oxygenation state transition of red blood cells using optical tweezers," Biophys. J. **96**(1), 209–216 (2009).
44. A. W. Jay and P. B. Canham, "Viscoelastic properties of the human red blood cell membrane. II. Area and volume of individual red cells entering a micropipette," Biophys. J. **17**(2), 169–178 (1977).
45. D. J. Faber, M. C. G. Aalders, E. G. Mik, B. A. Hooper, M. J. C. van Gemert, and T. G. van Leeuwen, "Oxygen saturation-dependent absorption and scattering of blood," Phys. Rev. Lett. **93**(2), 028102 (2004).
46. A. N. Bashkatov, D. M. Zhestkov, É. A. Genina, and V. V. Tuchin, "Immersion clearing of human blood in the visible and near infrared spectral regions," Opt. Spectrosc. **98**(4), 638–646 (2005).
47. B. R. Wood, L. Hammer, L. Davis, and D. McNaughton, "Raman microspectroscopy and imaging provides insights into heme aggregation and denaturation within human erythrocytes," J. Biomed. Opt. **10**(1), 014005 (2005).

1. Introduction

Light scattering from red blood cells (RBCs) is an important research problem and has been studied considerably. Many recent papers show that an osmotic environment, osmotic stress, or the healthiness of the cell affects the RBC's shape [1–4]. The deformability of RBCs is one of the significant factors determining the ability of the cells to change their shape when propagating in blood vessels and through tiny capillaries. It is important to know the size and shape of the cells when analyzing measurement results. The light scattering from the RBC depends on the shape, orientation, and volume of the RBC, as well as its refractive index, which depends on the hemoglobin concentration [5,6]. Polarization of the incident laser light also has clear effects on scattering patterns [5].

Different kinds of theoretical calculations, based on several methods, have been performed in an attempt to understand light-matter interaction at the cellular level [5,7–9]. Because of the biconcave shape and the ability of RBCs to deform, the cross-section toward an illuminating laser source varies. This variation makes it difficult to determine the exact mean cell volume [10]. Different spheroid and elliptical models have been developed for RBCs to facilitate interpretation of measurement results and also to make modeling easier [7,10–12]. The cross-section of the RBC will be different for stretched cells when the stretching occurs in two different orthogonal directions.

Flow cytometry, two-angle light scattering, Fourier transform light scattering techniques, as well as measurements using a photometer with photographic film as a detector have been used to study the optical properties of single particles [6,11,13–17]. Typically, isovolumetric sphering is needed to eliminate changes in orientation and shape [10] and, hence, this kind of system does not allow measurement of cells in different orientations. However, flow cytometry studies have demonstrated that changes in the RBC's shape and orientation affect light scattering distribution [11,13,14].

Optical tweezers have been used for manipulation and measurement more than twenty years in biological sciences [18–20]. Optical tweezers have been used a lot to study the mechanical properties of red blood cells [21]. Different configurations have been developed to manipulate the orientation of the particle in the trap. Two-beam and multiple-beam optical tweezers make trapping and manipulation of a cell's shape possible [21–26].

The group in [27] used optical tweezers to keep single cells still and used the same trapping laser to illuminate the cell and a linear diode array to measure light diffraction from the cells. Optical tweezers have also been combined with other measurement instruments, such as light scattering goniometers [28–30] and a Raman spectrometer [31]. In these studies, single cells and particles are kept still under the microscope objective with laser tweezers during the measurement. Light scattering studies of single particles have been used to verify theoretical models. Studies on different cells have concentrated on lymphocytes, A375 cells, and granulocytes [28,29]. It was found that light scattering from biological cells has significant and complex time dependence [28]. The scattering patterns also reveal differences in the cell's internal structure [28]. In all cases, convection flow in the cuvette has induced instability of the cell during the measurement [28–30]. Also other biological samples have been investigated using the total intensity of elastically scattered light [32] and an integrated

Raman- and angular-scattering microscope (IRAM) [33]. However, no scattering light distributions from the trapped objects as a function of the scattering angle were measured in paper [32], and the microscope's glass slides might affect the results of the IRAM system [33]. In addition, no optical tweezers with enough axial trapping force were combined with the IRAM system to control the orientation of the sample cell [33].

In this paper we demonstrate the usability of a setup consisting of optical tweezers with two optical traps combined with a light scattering measurement system. We show that it is possible to control the shape and orientation of a red blood cell and measure light scattering from red blood cells in different orientations and dimensions. We also show the results of scattering from a single spheroid RBC and compare them with signals from a 6.0 µm polystyrene sphere. We also discuss the effect of an osmotic environment on the RBC's shape and light scattering properties at the single-cell level. Differences between measurements and models as well as problems encountered in the measurements are discussed. The problem of the stability of the cell position during light scattering measurement is addressed by using two trapping beams. The results are discussed in relation to published simulation and experimental results found in literature.

2. Theoretical considerations

Normal human RBCs have a biconcave shape, their diameter is about 7-8 µm, and their thickness is about 2.5 µm [11,12,34]. The real part of the refractive index of erythrocytes at 633 nm is about 1.40-1.42, which is mainly caused by the combined refractive indices of oxygenated hemoglobin (1.615) and water (1.333) [35].

A tightly focused optical beam causes RBCs to rotate. The torque induces the cells to align parallel with the incoming laser beam in a position in which the integrated electric field within the volume of the RBC is maximized [23,25]. RBCs are also aligned so that their concave surfaces are in the direction of beam polarization, making it possible to rotate the cell by changing the polarization angle of the trapping beam [36,37]. Because of this alignment, the side wall of the cell can be seen with a CCD camera. RBCs can also be stretched with two separate beams. When a RBC is stretched, the shape of the surface of the leading edge changes. Changes in a RBC's shape have been measured and modeled earlier [21]. According to the data, a narrowing of 25% in one dimension of a RBC was estimated when the length of the cell increased 15% [21]. However, stretching of a cell is a bit different when using microspheres as handles in comparison with the case of trapping cells directly.

The Mie theory can be used to calculate elastic light scattering from spherical objects. MiePlot software [38] has been used in modeling. The following values have been used for a spherical RBC: diameter 5 µm and refractive index 1.4. For a 6.0 µm polystyrene sphere, the refractive index has been 1.59. This means the relative refractive indices are 1.2 and 1.05 for a polystyrene sphere and a RBC, respectively [39].

3. Measurement System

The construction of our double-beam optical tweezers system is shown in Fig. 1. We used a 1064 wavelength for trapping. The laser model was an ILM-L3IF-300 diode module (LeadLight Technology, Taiwan) with output power of 350 mW. After the laser unit, a beam expander was used to collimate the beam and extend the beam in order to slightly overfill the back aperture of the microscope objective. The beam was then divided into two different beams using a polarizing cube beam splitter (lower blue square in Fig. 1) [40]. A half-wave plate was placed before the cube beam splitter to control the optical power between these two beams. A telescope and the half-wave plate were placed in beam 1 after the first mirror. The latter lens in the telescope was attached to a mount that could be moved in a plane transverse to the beam axis. This allowed manual movement of the trap in the sample plane. The half-wave plate allowed optical power management with the upper polarizing cube beam splitter (upper blue square). Another half-wave plate was placed after the first beam splitter in beam 2

to control the optical power at the sample plane. A mirror in beam 2 was used to steer manually the other trap in the sample plane. We use a water immersion objective (Olympus LUMPLFL100XW/1.00) with a magnification of 100x and a working distance of 1.5 mm. The numerical aperture of the objective was 1.0, thus ensuring efficient trapping. A long working distance was needed to decrease He-Ne laser light reflection from the tip of the objective and its effects on our measurements. A dichroic mirror (Chroma) was used to guide the trapping laser light through the objective and allow the visible light from the sample to reach the CCD camera (LCL-902K, Watec America Corp.). Samples were measured in a 15-mm-high cylindrical cuvette (shortened version of Helma 540.115) with an inner diameter of 22.6 mm and an outer diameter of 25 mm. The sample chamber was placed on an adjustable sample stage, which was placed on a motorized xy stage (Thorlabs MAX201).
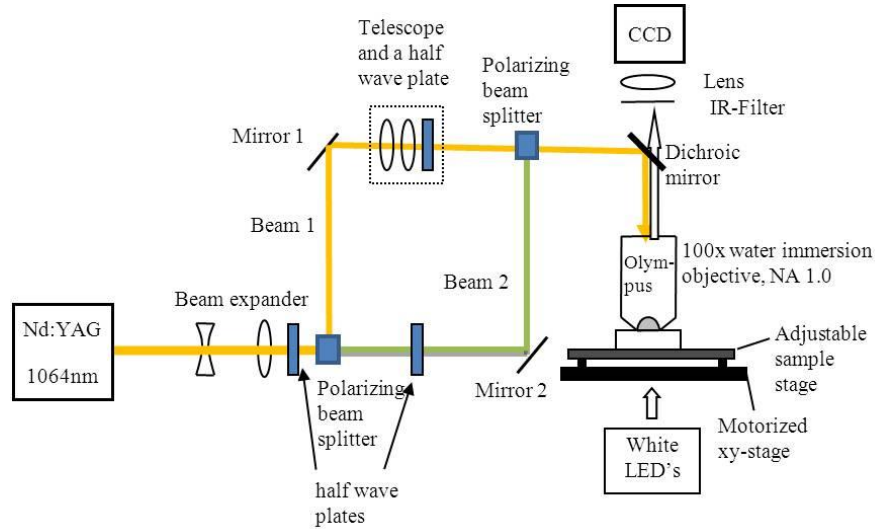
Fig. 1. Double-beam optical tweezers.

The setup for measuring light scattering on the illumination side consisted of a He-Ne laser (05-LHP-151, Melles Griot) with output power of 5 mW and a polarization ratio of 500:1, an optical chopper modulating the beam at a frequency of 76 Hz (Avesta), a focusing lens (+ 200 mm), and an aperture. On the detecting side, the setup consisted of three apertures, a lens on a steerable mount, an IR dichroic hot mirror (Thorlabs FM01), and an amplified photomultiplier tube (PMT) (Thorlabs PMM02). The voltage signal from the PMT was taken to the input of a phase-sensitive detection unit (Ortec Brookdeal, 9412A), and the chopped reference signal was taken to the input of the lock-in amplifier's reference unit (Ortec Brookdeal 9422). More details of the setup can be found in [30]. The detector was moved around the sample with a motorized rotation stage (Standa 8MR190-2-28, with 8SMC1-USBhF-B1-1MC controller). An angle step of 0.5° was used for the measurements. LabView 8.2 software was used to control rotation stage movement and for data acquisition. The scattering setup is shown in Fig. 2 (adapted from [30]).

The optical power of the He-Ne laser before the sample cuvette was about 2.8 mW. The output diameter of the laser beam was 2 mm, and the beam's focal diameter under the objective was calculated to be about 200 μm, which is enough for smooth illumination of a trapped particle. The polarization direction of the He-Ne laser varied in the measurements: part of the measurements were made with the polarization plane 22° from the vertical direction, and part with vertical polarization (0°). Polarization was changed by changing the orientation of the laser. The polarization angle was measured using a polarizing cubic beam splitter and a protractor. The polarization direction is given for each measurement result.
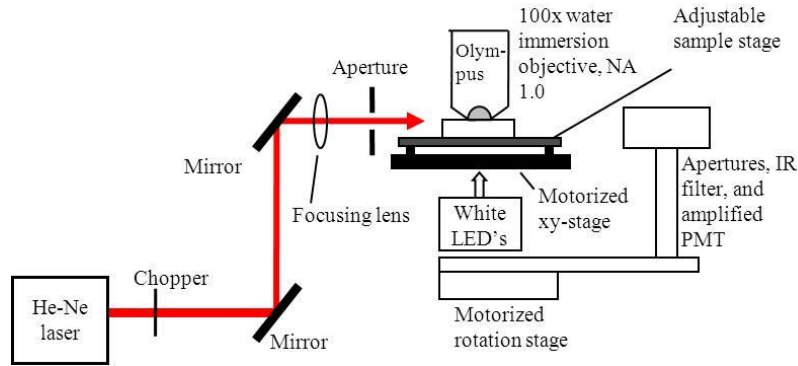
Fig. 2. Light scattering measurement system.

4. Alignment and measurement procedure

Before the measurements, the alignment of the setup was checked carefully. The procedure is described in detail in [30]. The measurements began by placing the cuvette under the microscope objective in the center of the beam so that the direction of light did not change. Then the particle or cell was trapped at the bottom of the cuvette. After that, the trapped object was carefully lifted up with a linear translation stage. When the object was in the same plane as the He-Ne laser light, if the cuvette was moved from its original position (if the cuvette changed the direction of the light), it was moved in the xy plane with the Thorlabs motorized xy stage. To maximize the light scattering intensity, the position of the particle inside the cuvette was fine-adjusted using the objective tilt adjustment screws. The white illuminating LEDs were switched off during the measurements. At each angle, the phase-sensitive detector was given five seconds (five times the time constant of the phase-sensitive detector) to stabilize. Thirty measurement samples were taken at a frequency of 10 Hz and then averaged.

When measuring red blood cells in different orientations, the cells were rotated using beam 1 and beam 2. This way we ensured that the optical power in both traps was approximately the same in the sample plane. The trap was moved in the sample plane by changing the angle of arrival of the beams to the objective's entrance aperture. This means that when the beam was moved away from its original position at the center of the objective entrance aperture, less light entered the objective and the optical power in that trap decreased. In cell elongation measurements the cell was rotated using both traps, but elongated by moving the beam 1 trap. This was done to prevent the cell from escaping from the trap during the elongation process. Each measurement of a cell took about 20 minutes. Two measurements were taken from each position or shape and also from the background to confirm the accuracy of the data. Even a single dust particle can cause an intensity peak or minimum in the measured curve. The measured data were processed with direct background subtraction.

5. Sample preparation

Fresh red blood cells were collected with the finger prick method and diluted with filtered PBS (phosphate-buffered saline, D8537, Sigma, Sigma-Aldrich). The PBS was filtered with a filter pore size of 0.2 μm (GELMAN Acrodisc 13 CR PTFE) three times. The cuvettes were carefully cleaned and filled with filtered PBS. A small amount (~10 μl) of cells were injected into the bottom of the cuvette using a pipette and allowed to sedimentate before trapping a cell for the measurements. The cell sedimentation process was a crucial part of the sample preparation which decreased the background signal of the measurements. All the samples were prepared and measured at room temperature.

Polystyrene spheres with known properties were used as a reference for comparison with the results from the RBCs. The cuvettes were carefully cleaned and filled with distilled water.

The water was filtered with a filter pore size of 0.2 µm (GELMAN Acrodisc 13 CR PTFE). A small amount of polystyrene spheres (6.0 µm, Bangs Laboratories, Inc.) were added to the water and the sample was allowed to sedimentate. After that, the upper part of the suspension was filtered again to reduce the background signal during the light scattering measurements.

A hypertonic solution was prepared using PBS solution and NaCl. The PBS solution was filtered three times using a 0.2 µm (PALL) filter. Approximately 74.5 mg of NaCl was added to 5 ml of PBS solution. This solution was then mixed well in a cuvette. The solution needed in the experiments was then taken from the top part of the mixture in the cuvette and filtered by using the 0.2 µm filter.

A hypotonic solution was made using PBS solution and distilled water; 2.5 ml of the PBS solution and 2.5 ml of distilled water were mixed in a cuvette. The mixed solution was filtered three times using a 0.2 µm (PALL) filter before it was used in the experiments.

6. Results and discussion

RBCs' ability to react to changes in the osmotic environment offer a good way to study light scattering by varying the refractive index and shape of the object. Figures 3 and 4 show that the refractive index of the particle has a clear effect on the light scattering intensity of the particle. Figure 3 (a) shows a scattering intensity image from a polystyrene sphere and Fig. 4 shows the measured intensity distribution from the sphere. Figure 3 (b) shows a trapped spherical RBC and 3 (c) shows the light scattering distribution under He-Ne laser illumination. Figures 3 (d) and (e) show corresponding images from a RBC in a hypertonic solution. The measured scattering signals are shown in Fig. 4, and this result is supported by findings from [3,6,41,46]. The authors in [3] found that, although the scattering cross-section decreases, the increasing relative refractive index is a dominating factor, and hence, overall scattering increases. The effect of glucose on the RBC is time-dependent, and an overall reduction in scattering was found to start after 20 minutes [42].

Three measurements were taken from a swollen red blood cell. The stability of the measurement system was good and the inset in Fig. 4 shows the repeatability of the measurements. One measurement took about 10 minutes, and hence, the cell remained stable during the whole 30-minute period.

Figure 4 shows theoretical curves fitted to the measurement results from a polystyrene sphere and a spherical RBC. The fit is good for the polystyrene sphere in the measured
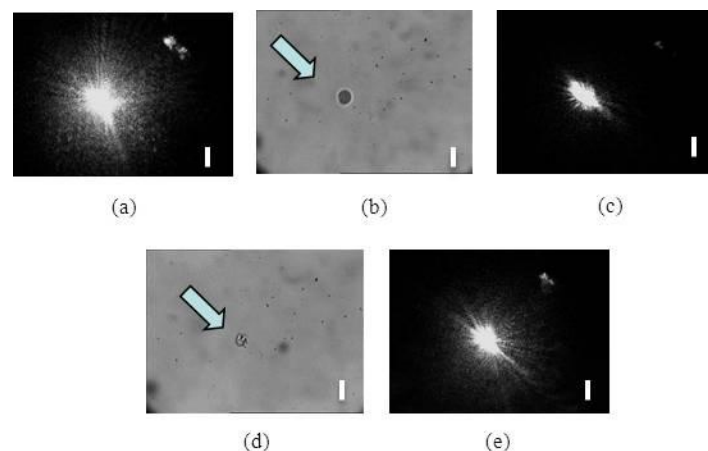

Fig. 3. CCD camera images from different trapped objects: (a) light scattering from a 6.0 µm sphere, (b) image of a swollen RBC, (c) light scattering distribution from a spheroid cell (in figure (b)), (d) image of an RBC in a hypertonic environment, and light scattering from the same cell (e). The arrow shows the direction of the incident laser light. Scale bar is 10 µm.
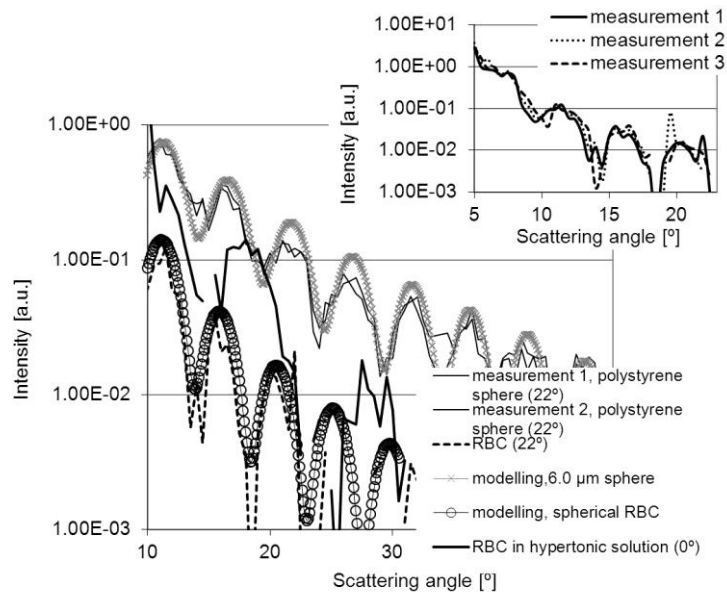
Fig. 4. Light scattering signal from a polystyrene sphere and a spherical red blood cell. The polarization directions of the incident He-Ne laser beam are shown in brackets. The thick black line depicts scattering from the RBC in a hypertonic suspension. Mie theory modelings of the polystyrene sphere and spherical RBC are included in the figure. The small inset shows the repeatability of the measurements during three different measurements.

angular range. Misalignment of the setup might induce some discrepancies between the measured and theoretical signals, which can be seen as a shift in the positions of the intensity minimums and maximums. Hence, careful alignment of the setup is important for the measurements. The cuvette walls may also induce changes in the measured signals if the position of the cuvette is not optimal and the He-Ne laser beam is tilted at the surfaces. However, these kinds of effects are in a minor role. In the modeling by Tsinopoulos *et al.* [5], plane wave incident light at 632.8 nm was used. They used a relative refractive index of 1.05 and expected that absorption inside the cell is negligible. We also found (Fig. 4) the same relative refractive index of 1.05 to be suitable for fitting the theoretical and experimental results for a red blood cell. However, osmotic effects may change this value, as demonstrated in Fig. 4.

Figures 5 (a) and (b) show the scattering distribution around the cell. It is possible to clearly see the intensity distribution in these figures, and in a wider angular range than in Fig. 6. The shape of the distribution is different for rim-on and face-on cases due to the different optical thicknesses of the cell as well as the distance of the cell membranes along the light path. The scattering cross-section is also different in those two cases. According to the simulations in Ref [7], scattered light appears to be significantly higher in the backward direction for face-on incidence than for rim-on incidence. Figures 5 (a) and (b) show that there is a slightly larger scattering signal in the backward direction in the face-on case than in the rim-on case when intensities are compared in relation to the cell surface.

Figure 6 shows light scattering patterns for a single RBC in rim-on and face-on orientations. It is clearly seen in Fig. 6 that in the rim-on case the distribution is wider than in the face-on case. Interference minimums and maximums are more clearly seen in the face-on case. Theoretical models have been made in order to understand this effect, and the main reasons are the thickness of the cell along the light path and the distance of the cell membranes, which induce a summation of signals in the larger angular interval in the rim-on
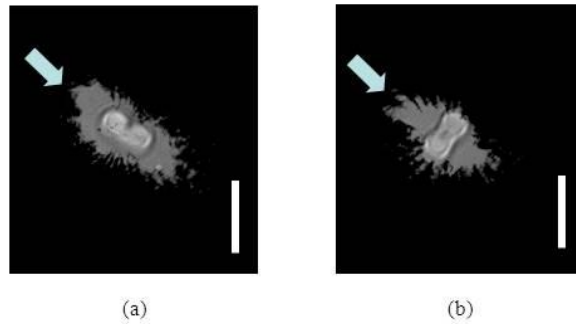
Fig. 5. Light scattering distributions from red blood cells in different orientations. Differential image of a cell in a rim-on case (a), and differential image of the cell in a face-on case (b). Arrows show the direction of the incident laser beam. Scale bar is 10 μm.

case and constructive and destructive interferences in the face-on case [5,8,9]. It must be noted that all the small images in Figs. 3, 5, and 7 show near-field distribution, but the measurements in Fig. 6 show far-field distribution. The measurements in Figs. 4, 6, 8, and 9 have been taken at the image plane and perpendicular to the trapping laser beam. Hence, the measured signals cannot be compared directly with the intensity images.

Modeling by Tsinopoulos *et al*. [5] showed that a spherical red blood cell is not a good model of the real shape of the cell. There are clear differences in the scattering patterns from a normal-shaped cell and a spherical cell. This is also seen in our measurement results in Fig. 6. Modeling by Nilsson *et al*. [7] showed that the forward-scattering peak is narrower and higher for an oblate spheroid at face-on incidence than for a sphere. This finding is supported by our measurements (Fig. 6), but this is not so obvious in Figs. 5 (a) and (b). Figure 7 shows RBCs in rim-on and face-on cases when the cell is stretched with optical tweezers. It can be seen that when stretching cells in the direction of the incoming laser beam (rim-on incidence), the scattering pattern does not change much. However, some changes can be seen in the face-on case.

Light scattering measurement results obtained with a goniometer for a stretching case with rim-on illumination are shown in Fig. 8. The smaller graph in Fig. 8 shows the repeatability of the measurements. One measurement took about 15 min and hence, the total time for two measurements was about 30 minutes. The light scattering distributions show that stretching
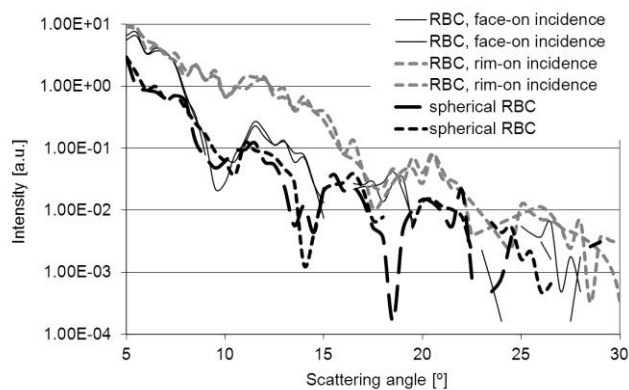

Fig. 6. Measurement results from a single RBC. He-Ne polarization was 22 degrees from the vertical position.

(a)   (b)   (c)   (d)
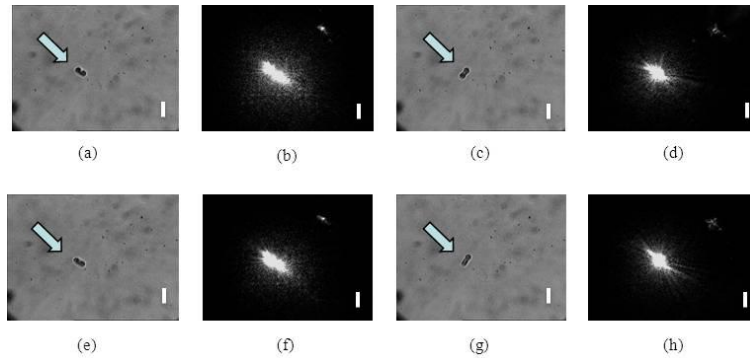
(e)   (f)   (g)   (h)

Fig. 7. Stretching of a RBC in a rim-on case (a,b,e,f) and a face-on case (c,d,g,h). Scale bar is 10 μm.
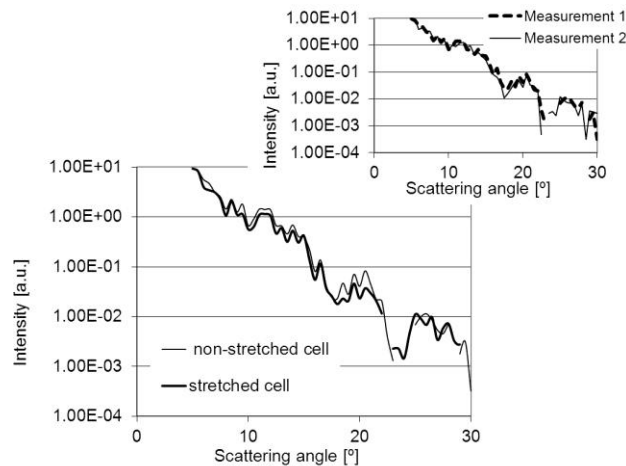

Fig. 8. Measured light scattering pattern from a stretched cell related to Fig. 7 (a,b,e,f) in a rim-on illumination case. The polarization direction of the He-Ne laser is 22°.

has a minor effect in the direction of the illumination axis. According to the simulations [7], forward scattering intensity should decrease when the ellipsoid elongates. This effect can't be seen from Fig. 8 because the straight light prevented us from starting the measurements from 0°.

Figures 7 (d) and (h) show light scattering intensity images in the face-on illumination case. Corresponding measured scattering distributions are shown in Fig. 9. Clear shifts in the positions of the peaks in the scattering pattern can be seen. The smaller inset shows the repeatability of the measurements during two separate measurements.

Theoretical reasons for the shifts and increased frequency of intensity maximums in Fig. 9 may originate from an increased cross-section of the cell in relation to the incident laser beam. The area-to-volume ratio increases due to folding [43]. Cell thickness along the light path may also change. Mechanical stretching has been found to also induce other kinds of effects that may change the scattering properties of RBCs. When the cell is under stress, elongation can decrease the internal volume of the cell when water and solutes come out [44]. This may result as a higher hemoglobin concentration and a larger refractive index. Rao *et al.* [43] found that stretching a RBC with a high oxygen concentration induced the cell to change its state into a deoxy state. Because the refractive index of oxygenated hemoglobin is higher than that of normal hemoglobin [45], stretching might decrease the refractive index of the cell. Scattering of whole blood has also been found to be stronger for oxygenated blood than for
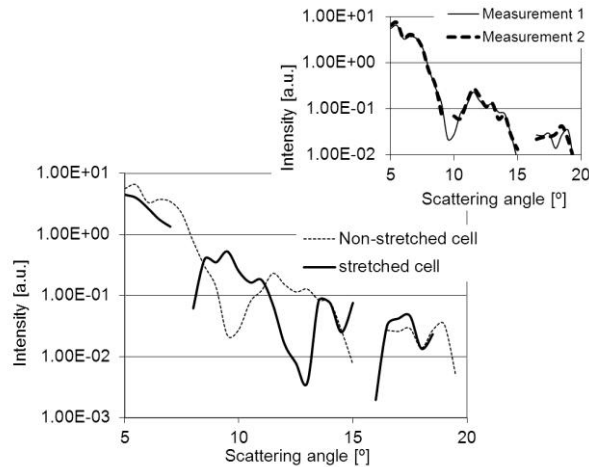
Fig. 9. Light scattering distribution from the stretched cell related to Fig. 7 (c,d,g,h) in a face-on illumination case. The polarization direction of the He-Ne laser is 22 °.

de-oxygenated blood. Those two effects are contradictory to each other. The anisotropy factor differs for oxygenated and de-oxygenated blood. This means that stretching the cell might increase the anisotropy value.

Size and shape may also change due to some diseases. Ergül *et al.* [4] measured scattering cross-sections and used a combination of forward scattering, backward scattering, and side scattering in their analysis to differentiate healthy and diseased cells from each other. They found that spheroid RBCs (spherocytosis) will result in a decreased scattering cross-section in the side-scattering direction. Shape has clear effects in the range of 5-30° (Fig. 6). It is clearly seen that a change in orientation has a larger effect than stretching. This is supported by the work by Nilsson *et al.* [7].

Earlier studies have discussed the scattering properties of cells in different orientations. They show that the orientation of the cell in the trap may have an effect on the measured scattering phase function [28]. When using only a single-beam trap, dynamic changes in cell orientation were found in the time scale of milliseconds to seconds [28]. We show in this paper that two traps are enough to stabilize and control cell orientation during the measurements. Figures 5-9 show changes in the scattering patterns when a cell is stretched or rotated. The smaller insets in Figs. 8 and 9 show that repeatabilities were good during the measurements (2 x 20 minutes). Our measurements support the findings in papers [1,5], where forward-scattered energy is dependent on cell orientation in the visible wavelength range. In addition to the single-cell-level light scattering models, our results also support the findings in papers [3,46], where increasing osmolarity increases scattering from a RBC when the size of the cell decreases and the refractive index of the cell increases. Friebel *et al.* [3] found a maximal scattering cross-section for shrunken RBCs. This is supported also by our results in Fig. 4. Roggan *et al.* [34] also found that RBC volume and refractive index, not shape, were the main factors in determining changes in scattering. Some articles describe cell heating and damage as well as two-photon excitation induced by optical tweezers [19,20]. Also laser-induced heme aggregation and denaturation have been reported [47]. However, Ramser et al. [31] demonstrated that trapping with irradiance of ~13 MW/cm^2 does not harm the cell. In our setup, irradiance in both traps was over two times smaller (due to the smaller numerical aperture and longer wavelength of the laser). He-Ne laser irradiation was also much weaker than in paper [47]. For that reason, these kinds of side effects are not considered to be a problem.

Our sample chamber had a diameter of 22.6 mm, which is very large for single-cell measurements. This kind of cuvette was used because it offers the possibility to use a water

immersion objective. A drawback originating from the large cuvette is the background signal in our measurements, which needed to be minimized. Due to the high background signal and the small relative refractive index of RBCs and PBS, we could only measure scattering patterns in the angular range of 5-30°. Polystyrene spheres have a higher refractive index than RBCs, and hence, the measurements were conducted in a wider angular range. Background reflections from the cuvette walls have appeared to be an error source in other experiments, also, but smaller cuvette dimensions have smaller light paths inside the cuvette, and the signal may be less affected by the immersion medium [28,29].

7. Conclusion

We demonstrated a two-beam optical tweezers system with a goniometric system with a detector to measure light scattering patterns from a single RBC in controlled orientations. Elastic light scattering was also measured from RBCs during stretching with a double-beam tweezers. Two beams were enough to stabilize the RBC cell position for the duration of the measurement. Good comparability with theoretical work was found. Scattering measurements with different osmotic environments at the single-cell level are in agreement with published results for whole blood.